

## QUANTUM OSCILLATOR UNDER EXTERNAL IMPULSE FORCE

Andrey L. Sanin<sup>1\*</sup>, Andrey T. Bagmanov<sup>2</sup>

<sup>1</sup>Department of Theoretical Physics, St. Petersburg State Polytechnical University, Polytekhnicheskaya 29,  
195251, St. Petersburg, Russia

<sup>2</sup>Independent researcher

\*E-mail: andreylsanin@yandex.ru

**Abstract.** In this contribution dynamics of quantum oscillator under external impulse force is investigated. The oscillator with symmetric polynomial potential in the well of impenetrable walls is considered. The potential consists of quadratic and cubic terms; the cubic term depends on modulus of coordinate. Influence of walls and anharmonicity on vibrations is discussed. Properties and peculiarities of resonances have been studied in context of non-stationary Schrödinger's equation at specified initial conditions. Solutions for the probability density, expectation coordinate as function of time; Fourier's spectra were analyzed in detail.

### 1. Introduction

The study of quantum wave packet dynamics under external force fields is of widespread interest in different areas of physics, optics, and informatics. External actions on quantum wave packet of a particle can excite resonant motions. Although the resonant problem is discussed in scientific literature, for example in [1, 2], it is investigated insufficiently. It is necessary to perform the comprehensive numerical calculations to open a new area in control of quantum states and quantum means. Here, the external action can be seen as controlling. In our previous paper [3] we studied the ordinary and parametric resonances for a spatially bounded quantum harmonic oscillator. At present paper, the polynomial bounded potential as a composition of quadratic and symmetric cubic terms is studied. The symmetric cubic term depends on coordinate modulus to the third power. The main topic of our paper is a classic resonance of oscillator under impulse force. Some results of the paper [3] will be represented and discussed in the context of main topics related to resonances and anharmonic properties. Notice that the notion "spatially bounded oscillator" was used in monograph [4] for description of the quantum harmonic oscillator in rectangular potential well with impenetrable walls. This notion will also be used by us for the description of anharmonic oscillator in the infinitely deep rectangular potential well.

### 2. Principal equations and assumptions

The dynamic of spatially bounded quantum oscillator is considered in domain

$$-L \leq x \leq L, \quad (1)$$

where  $x$  is coordinate located in  $[-L; L]$ . On domain boundaries the wave function  $\Psi(x, t)$  satisfies to the condition

$$\Psi(\pm L, t) = 0, \quad (2)$$

where boundaries are of the walls of an impenetrable well,  $t$  is time. In the domain, the quadratic potential is specified as

$$U = \frac{1}{2} m \omega^2 x^2 + k|x|^3, \quad (3)$$

where  $m$ ,  $\omega$  are mass and frequency of oscillator,  $k$  is constant, respectively. To set Cauchy's problem it is necessary to specify the corresponding initial condition

$$\Psi(x, t=0) = \Psi_0(x). \quad (4)$$

We consider two types of those conditions. In the first case, we use the wave function  $\Psi_0(x)$  for the ground state of quantum harmonic oscillator on the interval  $(-\infty, \infty)$ . Here, the wave function obeys to the equation  $\Psi_0 = A \exp(-x^2 / 2(\Delta l)^2)$ , the constant  $A$  can be obtained from the normalization condition

$$\int_{-L}^L \Psi^* \Psi dx = 1. \quad (5)$$

The normalization condition is complied with sufficient exactness in time for the investigated dynamic processes. In the second case for the spatially bounded anharmonic oscillator, the wave function  $\Psi_0$  is designed from the numerical solution of the stationary Schrödinger equation.

To describe the wave packet dynamics at conditions (2), (4) and the external action, the time-dependend Schrödinger equation is used

$$i\hbar \frac{\partial \Psi}{\partial t} = -\frac{\hbar^2}{2m} \frac{\partial^2}{\partial x^2} \Psi + U_\Sigma \Psi. \quad (6)$$

Here  $U_\Sigma = U + U_e$ ,  $U_e$  is the external potential,  $\hbar$  is the reduced Planck's constant,  $i$  is an imaginary unit. The transition to the non-dimensional quantities and operators in Eq. 6 can be obtained by means of the basic units of length, time and energy  $U_0$  as follows

$$\Delta l = \sqrt{\frac{\hbar}{m\omega}}, \quad \Delta t = \frac{m(\Delta l)^2}{\hbar} = \frac{1}{\omega}, \quad U_0 = \frac{\hbar^2}{m(\Delta l)^2}, \quad k_0 = \frac{U_0}{(\Delta l)^3}.$$

As results, we have

$$\zeta = x / \Delta l, \quad \zeta_L = L / \Delta l, \quad \tau = t / \Delta t, \quad \beta = k / k_0,$$

$$\tilde{U} = U / U_0, \quad \tilde{U}_e = U_e / U_0,$$

$$\frac{\partial^2}{\partial x^2} = \frac{1}{(\Delta l)^2} \frac{\partial^2}{\partial \zeta^2}, \quad \frac{\partial}{\partial t} = \frac{1}{\Delta t} \frac{\partial}{\partial \tau}, \quad \tilde{\Psi} = \Psi / (\Delta l)^{-1/2},$$

and the Schrödinger equation is written as

$$i \frac{\partial \tilde{\Psi}}{\partial \tau} = -\frac{1}{2} \frac{\partial^2}{\partial \zeta^2} \tilde{\Psi} + \tilde{U}_\Sigma \tilde{\Psi}. \quad (7)$$

The non-dimensional initial condition of the first type takes form

$$\tilde{\Psi}_0 = \tilde{A} e^{-\frac{1}{2}\zeta^2}, \quad (8)$$

where  $\tilde{A}$  is a non-dimensional constant. The normalization condition (5) can be rewritten as

$$\int_{-\zeta_L}^{\zeta_L} |\tilde{\Psi}|^2 d\zeta = 1. \quad (9)$$

The quantity  $\tilde{A}$  can be defined from (9). If  $\zeta \in [-20, 20]$ , then the quantity  $\tilde{A}$  is equal to 0.7511. This value is slightly distinct from the value on the interval  $(-\infty, +\infty)$ . The initial wave function  $\tilde{\Psi}_0$  tends rapidly to zero with increasing the coordinate  $\zeta$ .

By using the standard formulae for the probability density and probability stream density, in next analysis we introduce the non-dimensional probability density  $N$ , the non-dimensional velocity of the probability fluid  $V$  determined as follows

$$N = \tilde{\Psi}^* \tilde{\Psi}, \quad V = \frac{1}{2i} \left( \tilde{\Psi}^* \frac{\partial \tilde{\Psi}}{\partial \zeta} - \tilde{\Psi} \frac{\partial \tilde{\Psi}^*}{\partial \zeta} \right) / N. \quad (10)$$

The dimensional velocity of the probability fluid  $v$  can be defined from the relations  $V = v/v_0$ ,  $v_0 = \Delta l \cdot \omega$ .

The non-dimensional velocity operator can be defined as  $\hat{V} = -i \frac{\partial}{\partial \zeta}$ .

For dynamic analysis we shall also calculate the mean values of the coordinate and velocity by means of the formulas

$$\begin{aligned} \langle \zeta \rangle &= \int_{-\zeta_L}^{\zeta_L} \tilde{\Psi}^*(\zeta, \tau) \zeta \tilde{\Psi}(\zeta, \tau) d\zeta, \\ \langle V \rangle &= \int_{-\zeta_L}^{\zeta_L} \tilde{\Psi}^*(\zeta, \tau) \left( -i \frac{\partial}{\partial \zeta} \right) \tilde{\Psi}(\zeta, \tau) d\zeta. \end{aligned} \quad (11)$$

In separate cases numerical calculations of the normal variances  $\sigma_\zeta$ ,  $\sigma_V$  were carried out, which are determined as

$$\begin{aligned} \sigma_\zeta &= \left[ \int_{-\zeta_L}^{\zeta_L} \tilde{\Psi}^*(\zeta, \tau) (\zeta - \langle \zeta \rangle)^2 \tilde{\Psi}(\zeta, \tau) d\zeta \right]^{\frac{1}{2}}, \\ \sigma_V &= \left[ \int_{-\zeta_L}^{\zeta_L} \tilde{\Psi}^*(\zeta, \tau) \left( -i \frac{\partial}{\partial \zeta} - \langle V \rangle \right)^2 \tilde{\Psi}(\zeta, \tau) d\zeta \right]^{\frac{1}{2}}. \end{aligned} \quad (12)$$

The expressions in the quadratic brackets are known as the formulae for the mean-quadratic values of coordinate and velocity, respectively. Using the Fourier transform, we have been investigated the frequency spectra for the temporal dependences of  $\langle \zeta \rangle$  and other quantities. Fourier transform for  $\langle \zeta \rangle$  is designated via  $F_{\langle \zeta \rangle}(\Omega)$  where  $\Omega$  is the non-dimensional frequency in units of the oscillator frequency.

The non-dimensional form of the stationary potential distributed between two impenetrable walls is the sum

$$\tilde{U} = \frac{1}{2} \zeta^2 + \beta |\zeta|^3, \quad (13)$$

where  $\beta$  is a variable parameter. Potential (13) is symmetric curve with respect to the axis  $\zeta = 0$ . To find the eigenvalues  $\lambda$  and eigenfunction  $\varphi$ , the stationary Schrödinger equation

$$\left( -\frac{1}{2} \frac{d^2}{d\zeta^2} + \tilde{U} \right) \varphi = \lambda \varphi \quad (14)$$

was solved numerically by the method described in [5]. Below we discuss the wave packet dynamics when the external action is a periodic sequence of impulses of a short duration. The non-dimensional potential of impulse action is of

$$\tilde{U}_e = -\tilde{F} \zeta, \quad (15)$$

where  $\tilde{F} = F/F_0$ ,  $F_0 = U/\Delta l$ ,  $F$  is a classic force. The next sections will be devoted to resonances and anharmonicity (§§ 3, 4).

### 3. Bounded quadratic potential and resonances

Firstly, we discuss the eigenvalues of the Hamiltonian operator that represent the energetic spectrum. It is well known that the energetic spectrum of quantum harmonic oscillator is

equidistant; it follows from the solutions of the stationary Schrödinger equation. If the quadratic potential is bounded with the well walls, then the situation is changed. On the finite interval  $[-\zeta_L, \zeta_L]$ , the equidistance property can be approximately conserved with specified exactness to some value of state number  $i$ . In our calculations, for the spatial interval  $[-8\pi, 8\pi]$  this number is equal to 12, then the difference  $\Delta\lambda_i = \lambda_i - \lambda_{i-1}$  becomes depending on number  $i$ . We demonstrate this property on the shorter interval  $[-\pi, \pi]$ . The eigenvalues of non-dimensional energies  $\lambda$ , obtained from Eq. 14 at  $\beta = 0$ , presented in Table 1.

Table 1.

$i$	$\lambda_i$	$i$	$\lambda_i$	$i$	$\lambda_i$	$i$	$\lambda_i$
1	0.4998	2	1.5003	3	2.5105	4	3.5611
5	4.7082	6	6.0129	7	7.5157	8	9.2333
9	11.1687	10	13.3190	11	15.6796	12	18.2450

Here  $\lambda_1$  is close to the value of the ground state energy  $\lambda_0$  for a harmonic oscillator. The difference between the second and first levels is close to the frequency of harmonic oscillator  $\Omega=1$  in the interval  $(-\infty, \infty)$ , but with increasing  $i$ , influence of the walls on the energy spectrum is evident. For interval  $\zeta \in [-\pi, \pi]$  the spectrum is not equidistant, the distance between the neighboring energy levels increases with the number of eigenstate. The eigenstate function  $\varphi_1$  corresponding to the eigenvalue of  $\lambda_1$  was also calculated and then approximated by an analytical formula. The function  $\varphi_1$  describes the ground stationary state of the system; it is used as the initial condition for the analysis of the time-dependented Schrödinger equation (7). If the external action is absent, i.e.  $\tilde{F}=0$ , then the solution of the non-stationary Schrödinger equation shows that the probability density and other variables do not alter in time. However, if we switch on the external driven force  $\tilde{F} \neq 0$ , the dynamic variables will be dependent on time. Below, we explored the oscillatory regimes in the spatial interval  $[-8\pi, 8\pi]$ .

Let us consider the time duration of impulse action  $\Delta\tau = \pi/8 = 0.39$ . This quantity is equal to 1/16 of the vibration period for the undisturbed oscillator. The impulses are repeatable at intervals  $T_0 = 2\pi$ . The frequency of impulse repetition is equal to  $\Omega_e = 2\pi/T_0$  (in the non-dimensional form). The calculations were carried out for the sequence consisted of these impulses. We performed the calculations for one and then for three impulses of the external action at the different values of non-dimensional force  $\tilde{F}$ . For values  $\tilde{F} = 10/\pi$ ,  $\tilde{F} = 20/\pi$  the results of calculations are presented in Figs. 1-3. The action of a single impulse on the oscillator in the ground state (8) was investigated in context of calculations for the probability density, the phase trajectories that relate to the mean coordinates and mean velocities. Fourier spectra for these variables were also studied. For a time of impulse action with the duration of  $\Delta\tau = \pi/8$ , the mean velocity  $\langle V \rangle$  increases from zero to some value in accordance with the parabolic law and then the phase trajectory becomes elliptical. The displacement  $\langle \zeta \rangle$  from the center of well is 1.58 and maximal value of velocity also ranges up to 1.58. For the impulse time, the normalization condition (9) is varied over the interval  $(1 \div 2) \cdot 10^{-4}$  and then it is conserved with higher exactness. The Fourier spectra were studied on temporal interval  $[-\pi/8, 8\pi]$ , they content the basic frequency  $\Omega=1$  corresponding to the bounded oscillator period  $2\pi$ . This oscillation period is observable easily at the map of probability density levels. The probability density at  $\zeta = 0$ , as a function of time, changes with the period  $\pi$  as for a

harmonic oscillator on the interval  $(-\infty, \infty)$ . Fourier spectrum of this function is expressed by the spectral components at frequencies  $\Omega = 0, 2, 4$ ; intensities of the other components decrease rapidly with the rise of frequency  $\Omega$ .

The action of next impulses demonstrates the existence of resonance, which manifests itself as the growth of the oscillation amplitude. The numerical data represented by the graphs allow us to state that ordinary classical resonance takes place. In Fig. 1 the map of probability density levels is shown, the dark “snake” characterizes the more intensity but the light domains exhibit just the opposite, i.e. the smallness or zeroth intensity. The localization of probability density in the finite domain can be explained in the context of probability fluid motion [6]. The deviation of “snake” from initial position is increased with time. The time -dependent mean coordinate and phase portrait amplify the picture of resonance (Figs. 2 and 3). The oscillation amplitudes are increased almost linearly. Such behavior takes place only in the ordinary classical resonance. The amplitude of external action determined by the impulse height  $\tilde{F}$  operates the resonant process. The phase trajectory on the plane  $(\langle \zeta \rangle, \langle V \rangle)$  is generated by arcs of elliptical form and short crooked transitions. The trajectories of first type correspond to the motion of a quantum wave packet without external action, whereas the trajectories of the second type on transitions are defined by short impulses of an external action. The every next impulse of the external action places the trajectory in higher elliptical orbit. So, the energy of external action is injected into the oscillator. If the next impulse does not arise, then the trajectory closes and describes the oscillations with the same amplitude. The sign change of the external action impulse produces leap-like decreasing of the oscillation amplitude and return of phase trajectory on lower elliptical orbit (Fig. 4).

On the close examination for weak oscillations, the performed calculations and conclusions are agreed with properties of a quantum oscillator.

#### 4. Anharmonic oscillator in a well with infinite walls

Now consider the anharmonic oscillator located between two impenetrable walls with one wall at  $-\zeta_L = -8\pi$  and another at  $\zeta_L = 8\pi$ . As in the previous case, it allows us to decrease the influence of walls on the oscillations. Below, all the calculations are performed for the potential (13) with  $\beta = 0.1$ . The eigenvalues of non-dimensional energies  $\lambda$  are obtained from Eq. (14) at  $\beta = 0.1$  and presented in Table 2.

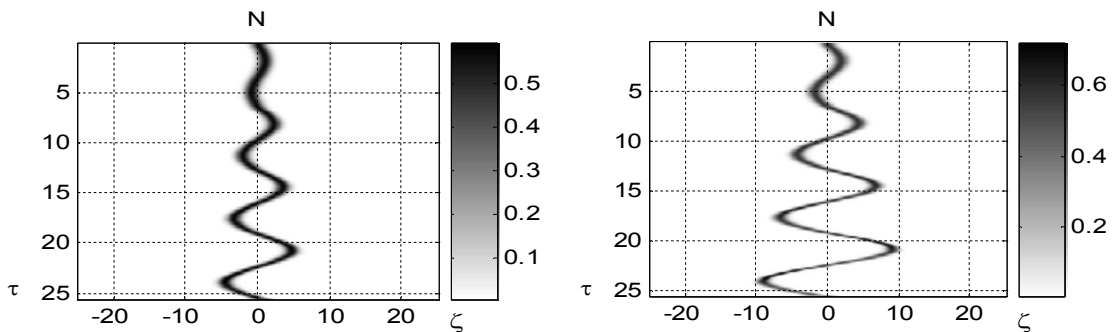
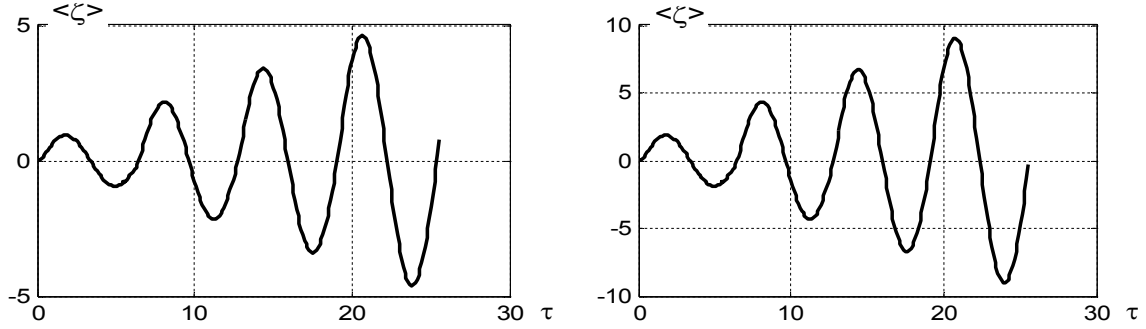


Fig. 1. Probability density as a function of time and coordinate.

a)  $\tilde{F} = 10/\pi$

b)  $\tilde{F} = 20/\pi$



**Fig. 2.** Mean coordinate as function of time.

a)  $\tilde{F} = 10/\pi$

b)  $\tilde{F} = 20/\pi$

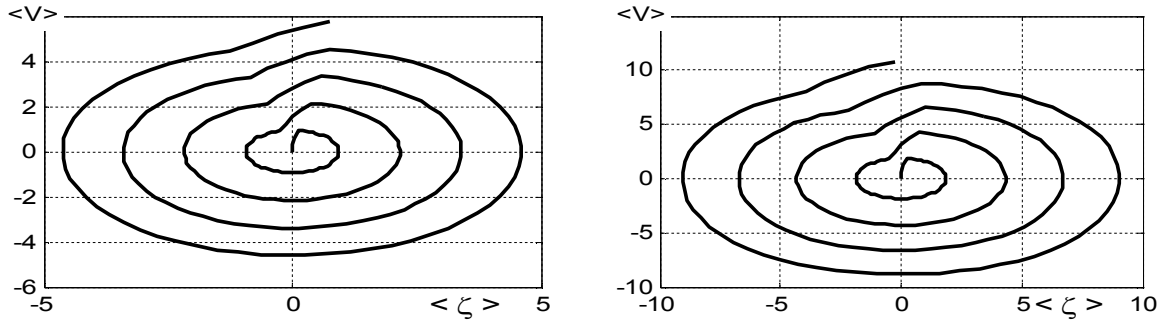


**Fig. 3.** Phase trajectories on plane  $\langle \zeta \rangle, \langle V \rangle$ . Parameters are the same as in Figs. 1, 2.

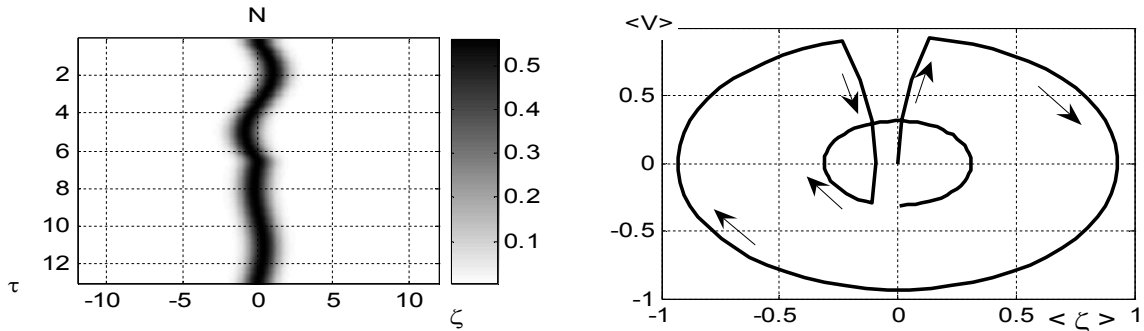


**Fig. 4.** Second impulse of opposite sign reduces oscillation amplitude.

a) Map of probability density

b) Phase trajectories

Table 2.

$i$	$\lambda_i$	$i$	$\lambda_i$	$i$	$\lambda_i$	$i$	$\lambda_i$
1	0.5504	2	1.6956	3	2.9042	4	4.1504
5	5.4282	6	6.7316	7	8.0577	8	9.4037
9	10.7679	10	12.1484	11	13.5442	12	14.9541

One can see that the difference  $\Delta\lambda_i = \lambda_i - \lambda_{i-1}$  increases with the state number  $i$ . In comparison with the stationary results for the quadratic potential on interval  $[-8\pi, 8\pi]$ , we have to notice the distinction. The distinction is caused by anharmonicity induced by the cubic potential. In spite of the growth  $\Delta\lambda_i$  with  $i$  for the quadratic potential on the narrow interval  $[-\pi, \pi]$  (see Table 1), the influence of cubic potential on dynamics can be more essential than the quadratic one. The eigenstate function  $\varphi_1$  corresponding to the eigenvalue of the background state  $\lambda_1$  was calculated and then was approximated by the formula

$$\varphi_1 = 4.5135 \cdot \exp\left\{-\zeta^2/2\right\} \cdot (a_0 + a_1\zeta^2 + a_2\zeta^4 + a_3\zeta^6 + a_4\zeta^8 + a_5\zeta^{10} + a_6\zeta^{12} + a_7\zeta^{14} + a_8\zeta^{16} + a_9\zeta^{18}) \quad (16)$$

where  $a_0 = 0.1715$ ,  $a_1 = 0.0088$ ,  $a_2 = -0.0019$ ,  $a_3 = 0.0005$ ;  $a_4, a_5, \dots, a_9 \approx 0$ . The coefficients  $a_i$  are written to the 4<sup>th</sup> sign after the point, at  $i \geq 5$  all the coefficient moduli are less than 0.0001. The calculations for time-depended solutions of the non-stationary Schrödinger's equation (7) were carried out at  $\tilde{F} = 10/\pi$ ,  $\tau = \pi/8$  with the initial condition (16), on the interval  $[-8\pi, 8\pi]$ .

We consider two modes of switching an external impulse force. In first case, the impulses of external force are switched on at specified time instants to obtain the maximum permissible rise of an oscillatory amplitude. These instants are  $\tau_1 = 0$ ,  $\tau_2 = 5.635$ ,  $\tau_3 = 10.85$ . The differences  $\tau_{i+1} - \tau_i$  allow as to find  $2\pi/(\tau_{i+1} - \tau_i)$  and compare them with corresponding  $\lambda_{i+1} - \lambda_i$ . The agreement between numbers can be quite sufficient. Such choice of instants is related with non-isochronous oscillations of the oscillator caused by a cubic non-linearity. At instant of time  $\tau = 11.2425$  the third impulse is switched off and the system is free from an external action. Under such method of oscillation excitement, the resonant mechanism is discrete in time, it is evolved to some instant of time, and then the oscillations stabilized. The map of probability density levels (values) on the plane  $(\zeta, \tau)$  is presented in Fig. 5. The more intensive values of probability density are pointed as dark and minimal values about some critical value have white or light gray colors. The expectation coordinate  $\langle \zeta \rangle$  on the interval  $[-8\pi, 8\pi]$  as function of time  $\tau$  is shown in Fig. 6. We can see that the quantity  $\langle \zeta \rangle$  increases with time in comparison with the initial value. The influence of anharmonicity at  $\beta = 0.1$  and  $\tilde{F} = 10/\pi$  consists in initiation of large-scaled envelope or modulation. The phase trajectories for expected values of  $\langle \zeta \rangle$ ,  $\langle V \rangle$  are plotted in Fig. 7. The solutions for  $\langle \zeta \rangle$ ,  $\langle V \rangle$  and phase trajectories correlate mutually. The map of levels for the probability stream density (8) also correlates with Fig. 5 for the probability density on the plane  $(\zeta, \tau)$ . The packet behavior can also be illustrated in frame of the normal deviation  $\sigma_\zeta$  as function of  $\tau$  (Fig. 9). The function  $F_{\langle \zeta \rangle}(\Omega)$  is of broadband peak, which can be related with the small time interval and also with system properties. In the second case, the external force impulses are switched on in equally spaced instants of time. The instants are  $\tau_1 = 0$ ,  $\tau_2 = 5.635$ ,  $\tau_3 = 11.270$ . The differences  $\tau_3 - \tau_2 = \tau_2 - \tau_1 = 5.635$  are the same. Here, the rise of oscillatory amplitudes takes place.

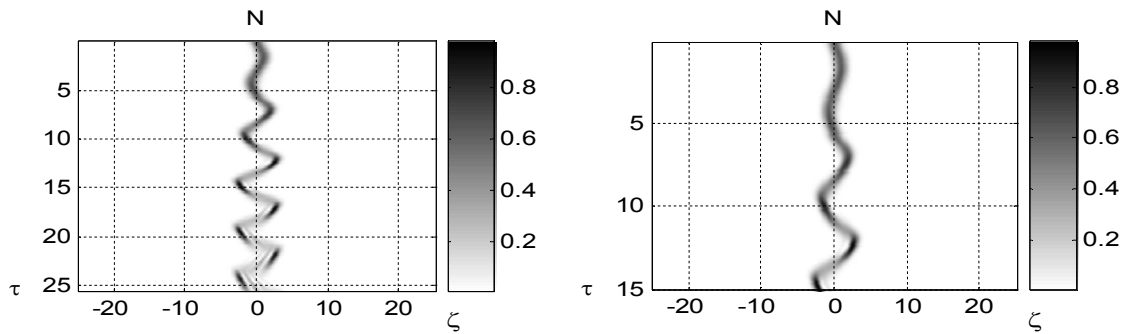


**Fig. 5.** The map of probability density values  
a) for  $\tau \in [0, 25]$  b) fragment for  $\tau \in [0, 15]$

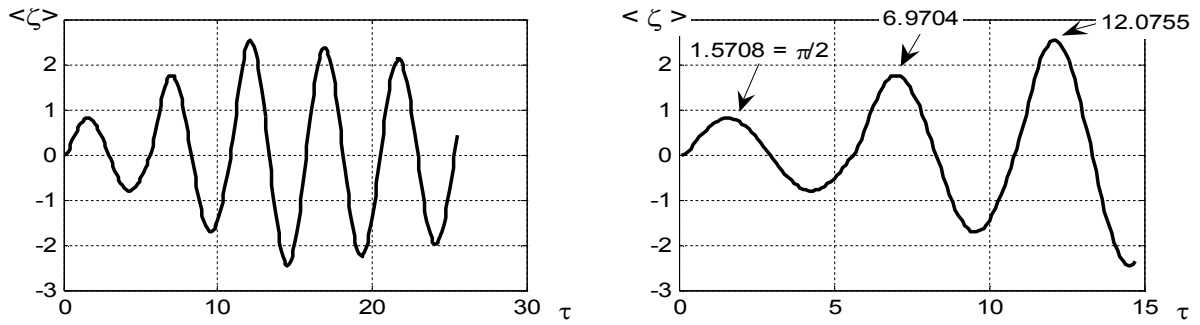


**Fig. 6.** Mean coordinate as a function of time.  
 a) for  $\tau \in [0, 25]$       b) fragment for  $\tau \in [0, 15]$

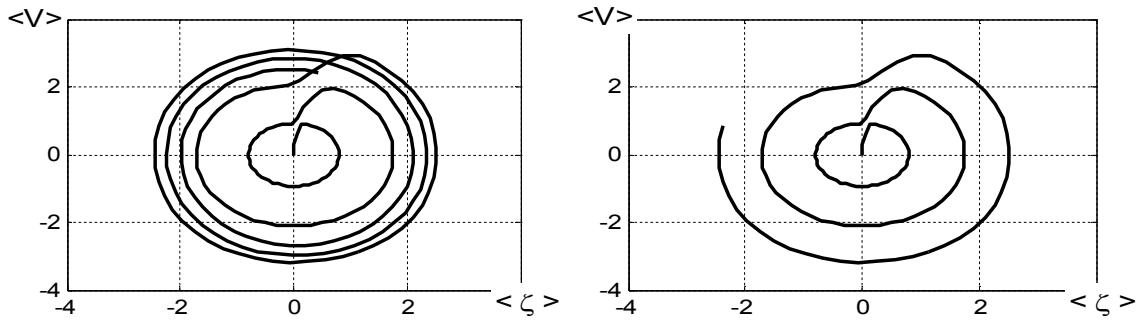


**Fig. 7.** Phase trajectories on plane ( $\langle \zeta \rangle$ ,  $\langle V \rangle$ )  
 a) for  $\tau \in [0, 25]$       b) fragment for  $\tau \in [0, 15]$

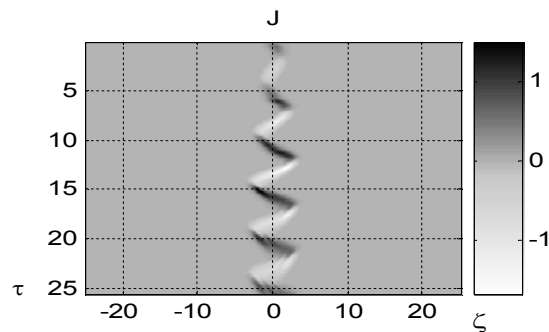


**Fig. 8.** Phase trajectories for a probability stream density.

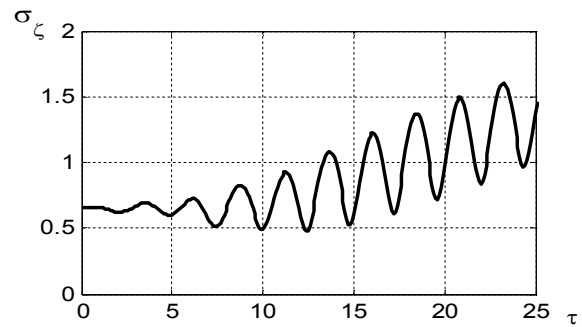


**Fig. 9.** Normal deviation  $\sigma_\zeta$  as a function of time.

The phase trajectories, Fourier spectrum, and the uncertainty product are represented in Figs. 10-12. The uncertainty product is the minimum at initial time of and then grows and oscillates. The probability density as function of coordinate at different times shown in Fig. 13 is subjected to a fragmentation, but at marked time instants the packet remains localized.

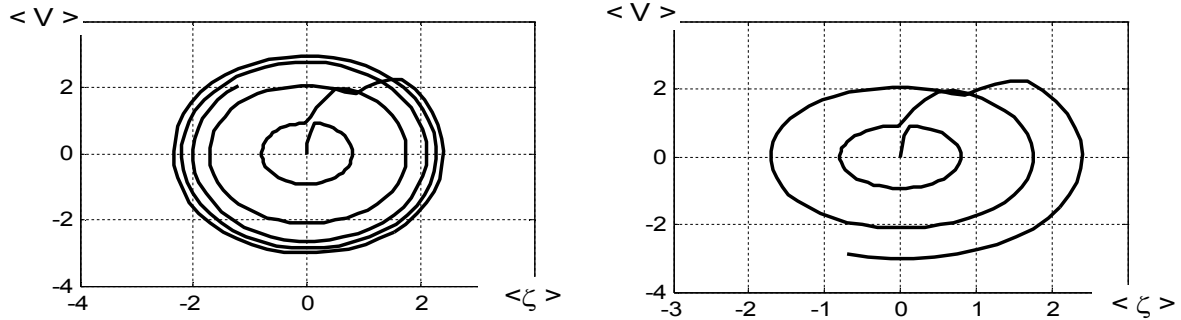


**Fig. 10.** Phase trajectories on plane ( $\langle \zeta \rangle$ ,  $\langle V \rangle$ ) under equally spaced external impulses  
 a) for  $\tau \in [0, 25]$   
 b) fragment for  $\tau \in [0, 15]$

We explored dynamic processes at small oscillations; the oscillatory amplitude was less than the well width. Nonetheless the anharmonicity influences on the properties, even though the impulse force is moderate and oscillations are weak.

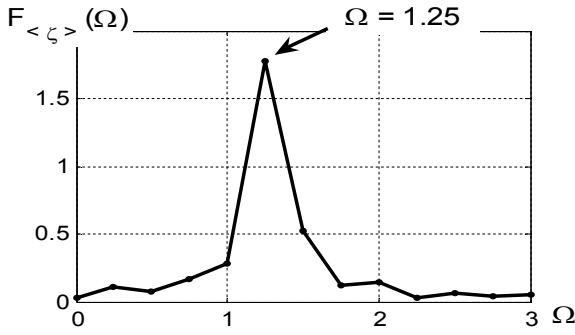


**Fig. 11.** Frequency response.

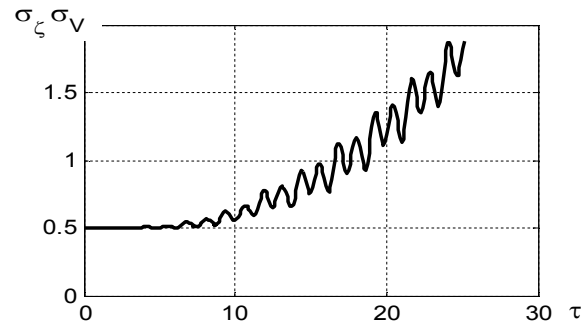


**Fig. 12.** Uncertainty product as a function of time.

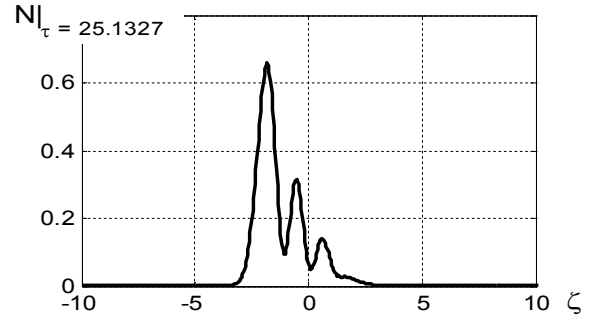
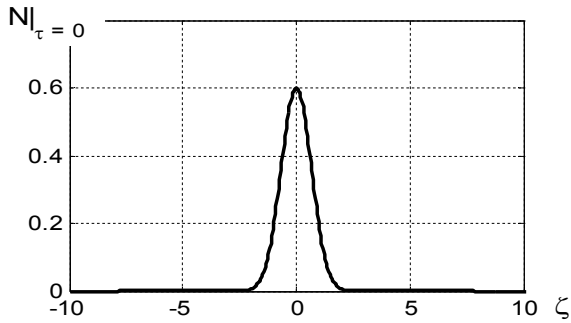


**Fig. 13.** Probability density as a function of coordinate at different times.  
 a) at  $\tau = 0$   
 b) at  $\tau = 25.1327$

### 5. Conclusion

The resonances of a quantum oscillator were investigated at the external impulse force. Resonant mechanism is evident for equidistant oscillator (the size of well is sufficiently large). It takes place if oscillator is not equidistant and influence of anharmonicity becomes essential. In our numerical calculations we chose the motion regimes when the influence of walls was weak.

### References

[1] A.B. Pippard. *The Physics of Vibrations. The Simple Vibrator in Quantum Mechanics.* (Cambridge University Press, Cambridge, 1983).

- [2] M. Latka, P. Grigolini, and B.J. West // *Phys. Lett. A* **189** (1994) 145.
- [3] A.T. Bagmanov and A.L. Sanin // *Uspechi sovremennoi radioelektroniki* No.12, (2005) 46.
- [4] N. Mott and I. Sneddon, *Wave Mechanics and Its Applications* (Clarendon Press, Oxford, 1948).
- [5] L. Juan, Uria van der Maelin, Garcia-Granda Santiago, Menendez-Velazquez // *Am. J. Phys.* **64** (1996) 327.
- [6] P.R. Holland, *The Quantum Theory of Motion* (Cambridge University Press, Cambridge, 1993).